DEMAGNETIZATION BY BASIN-FORMING IMPACTS ON EARLY MARS: CONTRIBUTIONS FROM SHOCK, HEATING AND EXCAVATION R. J. Lillis[1], S.T. Stewart[2], M. Manga[3], [1]UC Berkeley Space Sciences Laboratory (rlillis@ssl.Berkeley.edu), [2]Harvard University Department of Earth and Planetary Sciences, [3]UC Berkeley Department of Earth and Planetary Sciences.

Introduction: When a large hypervelocity impact occurs on a planetary body such as Mars, the kinetic energy of the impactor is partitioned primarily into 1) kinetic energy of the planetary crust and mantle as they deform and flow in response to the impact, 2) heating, melting and vaporization of impactor, crust and mantle material and 3) shockwaves that travel throughout the entire volume of the planet [1]. These processes demagnetize the crust by way of 1) excavation and rotation of magnetized material, 2) thermal demagnetization and 3) shock demagnetization respectively. A key element in understanding how large impacts demagnetize the crust is the manner in which magnetic minerals lose magnetization in response to elevated temperatures and pressures. At present, little is confidently known about which minerals may be dominantly responsible for the remarkably strong Martian crustal magnetic field [2]. The best candidates are (in rank order): magnetite, hematite, pyrrhotite, titanomagnetite and titanohematite [3].

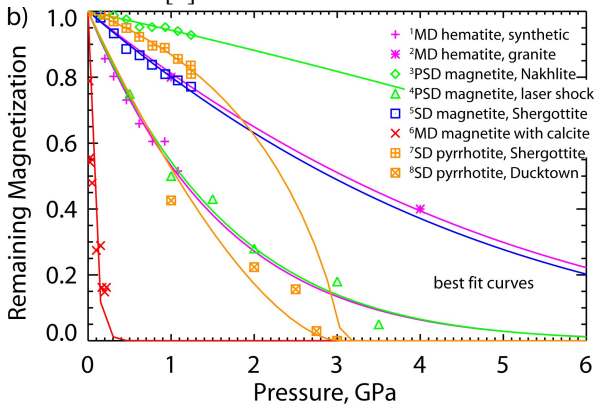

Figure 1: Experimental data sets for pressure-induced decrease of magnetic moment normalized to the initial magnetic moment, |M|, color-coded by magnetic mineral. The solid lines are the best-fits of our parameterization to this data.

Prior work on impact demagnetization at Mars has focused on estimating the peak pressure contours for specific basins and then comparing these to magnetic field measurements in order to place qualitative constraints on magnetic properties of the crust, acknowledging the uncertainty in the location of the contours, the non-unique relationship between magnetization and magnetic field, as well as the paucity of reliable shock demagnetization measurements of the primary candidate magnetic minerals.

Here we avoid scaling laws that are ill-suited to relating large basin topography to impact conditions and instead use hydrocode simulations to account for planetary curvature effects, deformation, melting, and excavation in order to better characterize removal of magnetization by 1) physical displacement, 2) heating and 3) shock pressure.

Parameterization of pressure-demagnetization. We use a simple 2-parameter function (a modified version of the cumulative distribution function of the gamma distribution) that is consistent with the large range of experimental pressure demagnetization data, whose curves range from very concave to quite convex [4] for different minerals and domain states.. Fits to 8 sample experimental data curves using this parameterization are shown in figure 1.

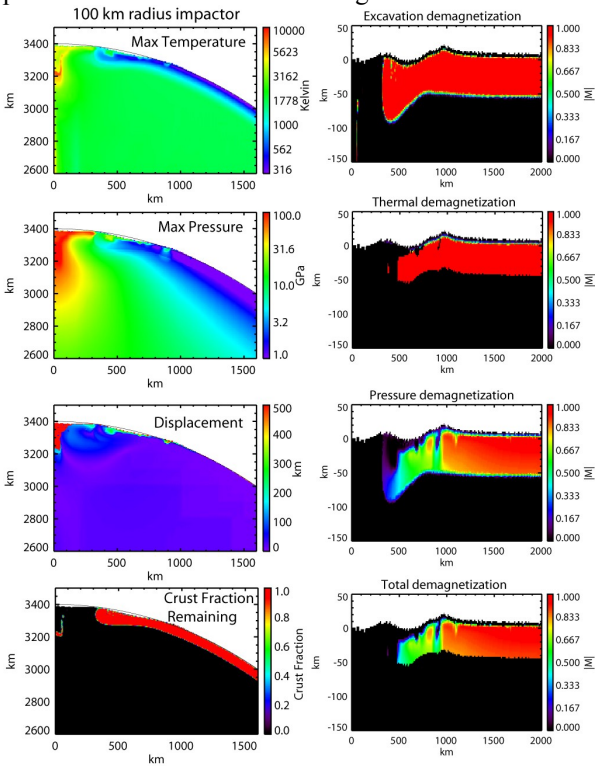

Figure 2: Left column shows maximum temperature, maximum pressure, displacement and remaining crustal fraction from a 100 km radius impactor. Right column shows the demagnetizing effects of excavation, heating and shock pressure, as well as total effects.

Impact simulations were conducted using the CTH code, a multi-dimensional and multi-material finite volume Eulerian shock physics code with second

order accuracy [5] that is widely used in planetary impact studies. The simulations use a fixed central gravity field. Simulations were performed for vertical impactor velocities of 10.6 km/s (corresponding to the vertical component of a 45º impact at 15 km/s) and impactor radii of 15, 25, 50, 100, 150, 200 and 250 km. The initial thermal state of the planet was guided by the crustal evolution calculations of Hauck and Phillips [6]. The left column of figure 2 shows the maximum temperature, maximum pressure, displacement and remaining crustal fraction from a 100 km radius impactor. 100 Myr of simulated post-impact conductive thermal evolution was then run to evolve the maximum temperature patterns.

Consequent demagnetization in 2 dimensions is calculated for a given blocking temperature and parameterized pressure-demagnetization curve, separately for excavation and thermal and pressure demagnetization separately, as shown by example in the right-hand column of figure 2.

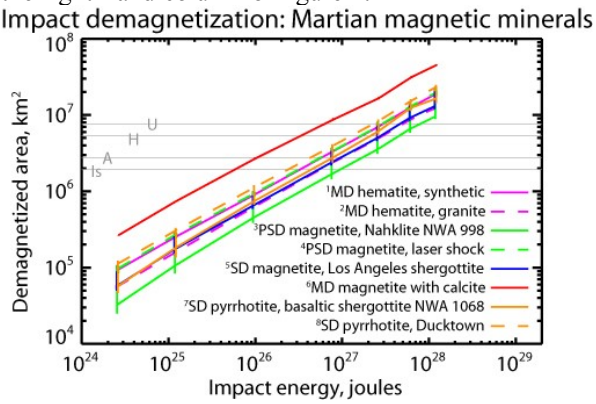

Figure 3: Demagnetized area is plotted as a function of impact energy for the 8 magnetic minerals shown in figure 1. Each color represents a different mineral: pink- MD hematite, green-PSD magnetite, blue- SD magnetite, orange-pyrrhotite. The light gray horizontal lines represent demagnetization areas for 4 of the large ancient impact basins on Mars: Isidis (Is), Argyre (A), Hellas (H) and Utopia (U) as determined by Lillis et al. [2010].

Results. For impacts of these scales, excavation and displacement are relatively unimportant for demagnetization compared with temperature and pressure effects. For the smaller impacts (15km and 25km radius impactors), pressure effects tend to dominate over thermal effects for plausible Curie temperatures and excavation is almost negligible. However, as impact size increases and more plastic deformation occurs, we see a non-negligible overlap between shock and thermal demagnetization. One mineral for which this m is the one of ay be true is single domain pyrrhotite (see figure 2), where a convex pressure-demagnetization curve and a Curie temperature of 325° C may lead to more thermal than shock demagnetization around 325 km from the impact point for the 50 km impactor and 500 km from the impact point for the 100 km impactor.

We may also use this framework to constrain the total demagnetized area as a function of impact energy for specific candidate Martian magnetic minerals. For each of our 8 sample pressure-demagnetization data sets and the best fits to those data sets, we calculate the total demagnetized area for each of our 7 impact energies, as shown in figure 3. The substantial range in demagnetized area for a given impact energy among our sample of candidate Martian magnetic minerals reflects the diversity of behavior with respect to shock pressures shown in figure 1. For example, the demagnetized area of the Argyre impact could be caused by impact energies ranging from 10^{26} J to ~1.5 x 10^{27} J (impactor radii of 50 km to ~125 km in our simulations). Similarly, the range of possible impact energies for a basin with a given demagnetized area is approximately an order of magnitude across the range of plausible magnetic minerals.

Unfortunately, due to the substantial variation of pressure-demagnetization characteristics across even different samples of the same mineral, even if we posit a single mineral type as the dominant magnetization carrier in the Martian crust, we are still left with a factor of several uncertainty in the possible energy of a given impact. Conversely, if we posit a specific energy for a known impact, we can constrain the pressure-demagnetization curve reasonably well but, with current information, we will be left with some uncertainty in the dominant magnetic mineral(s).

Looking forward. The techniques developed here would be greatly complemented by establishing an impact basin scaling law for Mars, i.e. a relationship between basin topography (of the surface and/or Moho) and impact energy. This would allow useful constraints to be placed upon the pressure-demagnetization properties of the dominant magnetic carrier(s), i.e. we could determine which of the curves in figures 1 and 3 correspond to the Martian case. When combined with a) extending the range of pressure demagnetization experiments and b) petrologic constraints from remote sensing of exposed surface minerals and/or meteorite studies, we could then expect to identify the likely primary magnetic mineral(s) and domain state(s) on Mars with some confidence. A corollary is that if the dominant magnetic mineral is known, these techniques can be used to verify the numerical models and associated basin scaling law.

References: [1] Melosh H. J. (1989), Oxford press. [2] Acuña M.H. *et al.*, (1999) *Science* 284, 790-79, [3] Dunlop J. and Arkani Hamed J (2005), JGR, 110, E12S04, [4] Louzada K. L. *et al.* (2011), *EPSL* 305, 257-269. [5] McGlaun et al. (1990), *Int. J. Impact Eng.*, *10*, 351-360. [6] Hauck S.A. and R.J. Phillips (2002), JGR *107* (E7), 5052